# Experimental study of Moment sharing in Multi-Joist Timber-Concrete Composite floors From Zero Load Up To Failure

J. Mudie [1c], W. M. Sebastian [2], J. Norman [1], I. P. Bond [1]

[1] Department of Civil Engineering, University of Bristol, University Walk, Bristol, BS8 1TR, UK

[2] Dept of Civil, Environmental and Geomatic Engineering, University College London, Chadwick Building, Gower St, London, WC1E 6BT, UK

## ABSTRACT:

The critical T-sections of multi-joist timber concrete composite (TCC) floors must be designed at ultimate for support shear force and midspan moment, both of which are influenced by transverse sharing, but to different extents. Prior experimental work has investigated only support reaction sharing and only up to serviceability loads. The present experimental study builds on that status quo by quantifying also moment sharing, via strain gauge layouts at ¼-span and midspan, along with reaction sharing via load cells at the supports of a multi-joist TCC specimen, over the entire load range up to failure. Use of steel mesh connectors bonded into hardwood laminated veneer lumber joists, and near geometric resemblance to a real building TCC floor recently built in London, were novel features of the specimen. The results show that midspan moment and reaction sharing both vary nonlinearly with load, but in distinctly different ways from each other (with up to almost 20% difference observed between them), in the progression between the uncracked, cracked and connection ductility regimes. In this approach reliable assessment of moment sharing depends on the quality of the recorded strains. Accordingly, the strain data were shown to be of high quality by converting these data to internal stress resultants that were then found to satisfy longitudinal equilibrium. It is concluded that this strain gauge layout is useful for future work aimed at building a database of transverse sharing of moments in TCCs.

**KEYWORDS:** timber concrete composite; indeterminacy; experiment; transverse distribution; hardwood; beech; LVL

[c] Corresponding author email address: joshua.mudie@bristol.ac.uk

# 1 Introduction

A timber-concrete composite (TCC) member comprises a timber joist or panel shear-connected to an overhead concrete slab. The connectors resist separation and slip between the timber and the concrete and generate shear forces along the interface, by these means significantly increasing the strength and stiffness of the floor relative to the case where the slab simply rests on the joist. TCC floors in buildings typically comprise concrete slabs continuous across multiple joists, an example of which is shown in Figure 1(a), and therefore there will inevitably be load sharing between individual composite T-sections, such as the one highlighted in Figure 1(a). In this paper, load sharing refers to two key behaviours, namely the sharing of reaction between individual joists at each support and the sharing of bending moment between individual composite T-sections at any section away from the supports and particularly at mid-span.

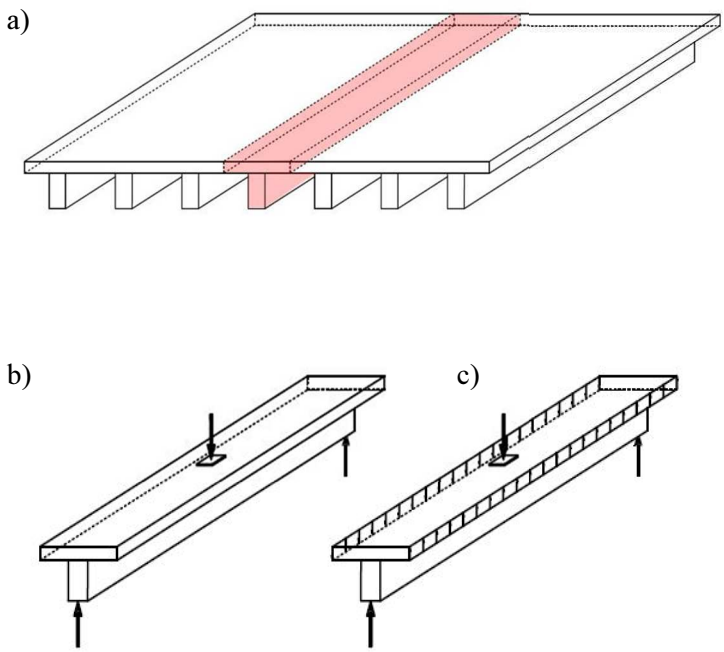


*Figure 1 - (a) TCC floor with a single slab spanning multiple timber joists, (b) isolated T-section, (c) isolated T-section with corresponding shear forces along the interfaces*

Now, it is convenient and sensible to isolate a single T-section for design against critical moment and shear force, as shown in Figure 1(b). What occurs in reality however, is shown in Figure 1(c), with vertical shear forces present along the imaginary vertical cut faces in the slab between T-sections. Due

to these **vertical** shear forces, in general moment sharing between T-sections at any section away from the supports will not mimic the corresponding support reaction sharing.

Notwithstanding this disparity between moment and reaction sharings, the approach in Figure 1(b) would be justified if the lower bound theorem of plasticity applied, which in itself is crucially dependent on sufficient ductility in the structural system. However TCCs in reality often show a behaviour which is brittle or of limited ductility. Hence any disparities between support reaction and midspan moment sharing cannot be overlooked and instead must be investigated as a crucial issue in their own right. The outcome of such an investigation can lead to even more effective use of the Gamma Method in Annex B of Eurocode 5 [1] as a design tool for TCC floors.

Research to date, e.g. [2-8], has focused predominantly on single-joist, single span, simply supported TCCs, which are internally indeterminate due to slab-joist slip. Another study [9] experimentally investigated the non-linear load responses up to failure of multi-span continuous, single T-section TCCs which, in the longitudinal direction, were both internally and externally indeterminate. In practice, TCC floors to date are largely simply supported with slab continuity in the transverse direction over multiple timber joists. It is the associated transverse indeterminacy which introduces the above challenge of quantifying load sharing, which has been investigated only in few previous experimental studies, including those by Monteiro [10] and by Kieslich and Holschemacher [11] who focused on support reaction sharing in the elastic regime of TCC behaviour.

In advancing these studies into the domain of midspan moment sharing from zero load to failure, two key considerations must be taken into account, namely the dimensional proportions and composition of the multi-joist TCC experimental specimens. To those ends a study of previous experimental TCC research shows that the span:depth ratio of the test specimens varied from 6.4 to 22.8, with the majority in the 13 – 18 range and with the spans in the 2m – 10m range. The average joist depth was 270mm, with slab thicknesses in the 30mm – 150mm range and an average of 65 mm. Joist spacing (or concrete slab width in single-joist specimens) ranged from 300mm to 2000mm with an average of 740mm [3-8,9,12-17,25].

Moreover the engineered timbers used previously have typically been softwood glulam, commonly spruce, with other studies using hardwoods [9,18], cross-laminated timber (CLT) [19] or laminated veneer lumber (LVL) [20]. The slabs have largely been of normal concrete, with a small number of studies using lightweight [21], cork-aggregate [22] concrete, limecrete [23], and fibreglass-strengthened concrete [24]. The most common timber-concrete shear connectors have been dowels, rods, or inclined screws affixed into the timber, with concrete cast around them [3, 5, 9, 25-27]. They are characterised by low slip stiffness and low ultimate strength, but good ductility. Glued connections [28] and notches cut into the timber joist [24-26] are significantly stiffer, yet suffer from lack of ductility. Expanded steel mesh and plates [29-33] have been used largely in softwoods and exhibit high stiffness compared to other connection types, with a good shear force-slip ductility plateau and high strength.

In cognisance of the above studies, the investigation reported in the remainder of this paper has incorporated a number of novelties to enable in-depth investigation of load sharing in multi-joist TCC floors. The key innovations embedded in this investigation were:

- The combination of *steel mesh connectors* and *laminated veneer hardwood* joists in a large-scale experimental multi-joist TCC specimen.
- Experimental quantification, from zero load to failure, of *moment* sharing across T-sections in this multi-joist specimen, based on implementation of an ad-hoc strain gauge layout on the specimen.
- Understanding the extent to which the nonlinear variations, with load, of moment and support reaction sharing are distinct from each other across the *entire loading range* up to failure.
- Demonstrating that the recorded strains which underpin the above assessments are reliable, by showing that the internal stress resultants based on these strains very nearly satisfy equilibrium.

To those ends, the following sections of this paper describe the details and testing of the large-scale multi-joist timber-concrete composite floor specimen used to investigate the above points. Also described are the double shear specimens fabricated to enable characterisation of the longitudinal shear behaviour of the connections. The test results are then presented and interpreted to provide new insight into moment and reaction sharing as nonlinear functions of load up to failure.

## 2 Materials and Methods

The details of the present specimen were partly influenced by the design of TCC floors constructed in multiple storeys of a new building in London in 2018 over 6m spans, using beech LVL joists spaced at 950mm centres, a 95mm thick concrete slab, and high shear stiffness coach screw connectors. The present specimen was of similar specifications, namely a 4.9m span, beech LVL joists at 700mm centres, an 80mm deep slab and expanded steel mesh shear connectors of very high stiffness, high strength and good ductility as shown in Section 3.5.1. Also, the use of hardwood enabled ductile connection behaviour to become manifest before final failure by flexural fracture of the timber.

In what follows, the design and fabrication of the experimental specimens is addressed, alongside the creation of a testing regime that addresses the key objectives, namely to:

- Understand the nonlinear variations, with load up to failure, of moment sharing and reaction sharing.
- Determine the effectiveness of the steel mesh plate connector in multi-joist TCC floor specimens.

A novel instrumentation layout was implemented in the specimen to enable inference of moment sharing at ¼ - span and midspan. That this moment sharing varied with load, as will be seen in Section 3.1, required the testing regime to record data right up to failure of the floor specimen, something which has not been previously pursued in the experimental domain for a near full-scale specimen. Due to limitations of space, logistics, and time, one full scale specimen was fabricated and was comprehensively instrumented.

### 2.1 Double shear push-out tests

Double-shear tests were performed in order to define the stiffness, strength, and ductility of the steel mesh-based connections. As shown in Figure 2, each connection specimen comprised a 120 x 240 x 600mm GL70 type S LVL joist connected on each side to a 625 x 300 x 80mm RC32/40 concrete slab with a layer of A193 steel reinforcing mesh (7mm diameter at 200mm square centres) at mid-depth to serve as anti-crack reinforcement during curing of the concrete.

Between the timber joist and the concrete slab a 19mm thick timber interlayer, which comprised thin layers of GL70 timber around a plywood core, was placed to serve as permanent formwork, thus further mimicking site practice. Tests to date on other TCC connections have found that the presence of an interlayer leads to significant reductions of slip stiffness and longitudinal shear strength. The interlayer was expected to be beneficial in the multi-joist floor tests due to its contribution to bending strength, but its impact on connection behaviour was less clear. Visual forensics were employed after the test to determine whether the interlayer acted as a soft medium that allowed the connector to fail within that interlayer, or whether it provided sufficient restraint to prevent buckling of the connector.

One steel mesh panel, 400mm x 100mm in elevation and fabricated from 10-09G pre-galvanised expanded steel mesh, is shown in Figure 3(a). Each TCC connector comprised two such panels, inserted side by side into each of two preformed grooves in the timber joist, as shown in Figure 3(b). Therefore, each connection in the main TCC multi-joist specimen contained four steel mesh plates.

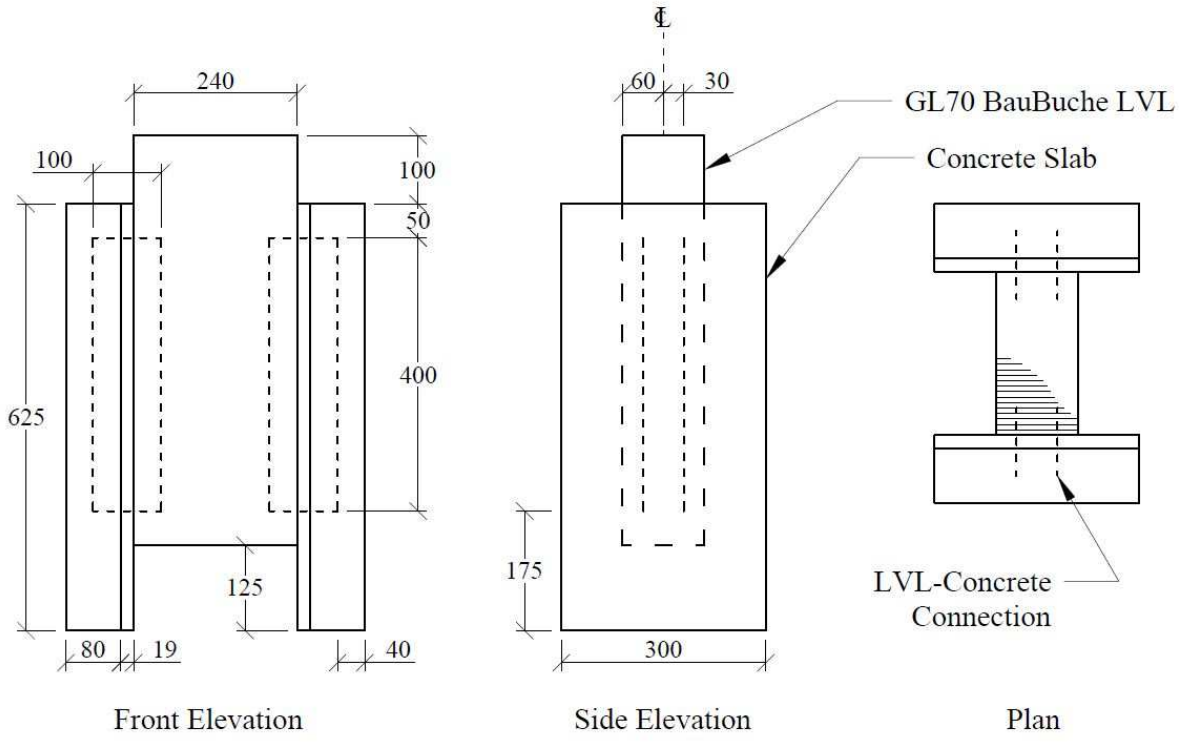


*Figure 2 - Dimensions of the push-out double shear specimens*

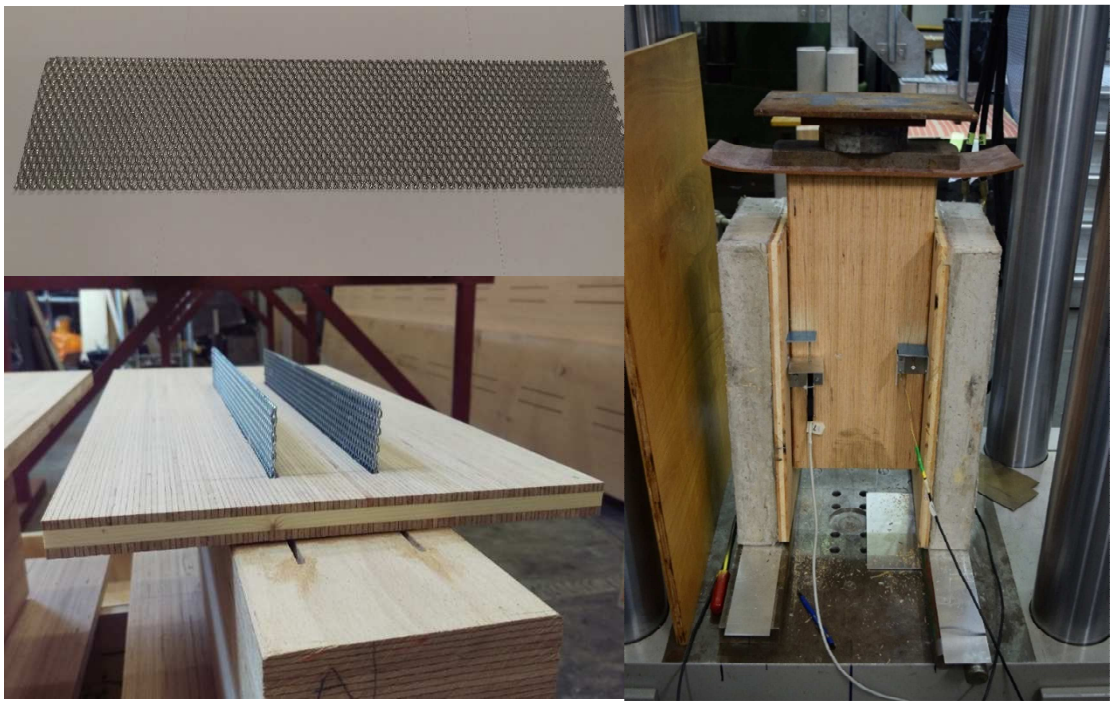

*Figure 3 – (a) mesh connectors, (b) connectors inserted into LVL joist, (c) double-shear specimen ready for testing.*

The specimens were tested in a DARTEC 600 kN testing machine, according to the procedure as defined in BS EN 26891 [34]. Force was recorded by the machine's internal load cell, while timber - concrete slip was recorded by four linear potentiometers aligned with the centres of the connectors, adjacent to each concrete slab on both sides of the joist. The two readings for each connector were averaged to allow for possible unsymmetrical behaviour. Figure 3(c) shows a specimen ready for testing.

## 2.2 Full-scale specimen

The aim of the large experimental specimen was, from zero load to failure, to enable understanding of the midspan moment and support reaction sharing capabilities of TCC floors, alongside determining the effectiveness of steel mesh plate connectors bonded into hardwood LVL joists in such floors. In order to enable inference of the moment sharing, it was crucial to devise an appropriate strain gauge layout. As shown in Figure 4, the presence of strain gauges at 3 distinct levels within the timber joist

allowed the assumption of a through-depth linear strain distribution to be checked and also enabled quantification of the joist's curvature at the gauged section. In order to check curvature compatibility between the concrete slab and the timber joists, strain gauge readings were also required from two further distinct levels within the slab. However, due to the presence of the formwork interlayer and to the small size of the steel mesh reinforcing bars this was not possible and only one longitudinally oriented gauge was placed on top of the slab.

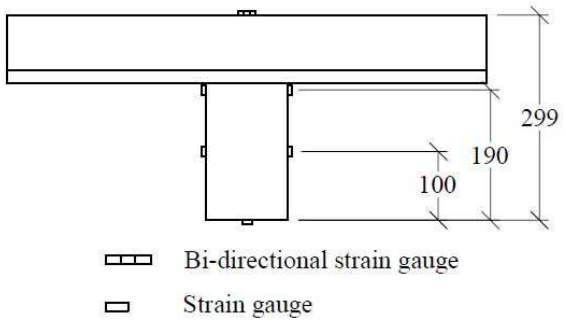


*Figure 4 - Through-depth strain gauge layout on TCC specimen*

The specimen consisted of three 120 x 200 section x 4900mm long GL70 type S LVL joists, spaced at 700mm centres, with slab overhangs such that each individual 'T-section' also had a slab flange width of 700mm. A 19mm thick interlayer (BauBuche Panel X) separated the joists from an 80 deep x 2100 wide x 4900mm long concrete slab, to the same steel mesh plate connector specification as for the double shear tests. Again, an A193 steel reinforcing mesh (7mm diameter, 200mm square spacing) was positioned at the mid-depth of the slab to prevent shrinkage cracks. A cross-section and elevation of the specimen are shown in Figure 5. The span:depth ratio of 16.3 sits comfortably within the spectrum of span:depth ratios of previous research TCC specimens as discussed earlier in the introduction, and the dimensions of both the joists and slab fall within the respective previous ranges presented also.

A conservative layout of connectors was chosen which, it was estimated, would allow the structure to take significant load, whilst still exhibiting ductility towards failure. The suitability of the connector layout was determined using a longitudinal shear analysis and estimates of the strength and stiffness of the connectors, which were then verified through the above-described double shear tests: a simple FE grillage model of the structure (formed of line-beam elements representing the three individual T-

sections, connected by transverse elements representing the concrete slab) was made, and a load applied under linear-elastic conditions. The shear forces from this model were converted to longitudinal shear at the interface via the equation $q = \frac{VA\bar{y}}{I}$ and compared with the shear capacity of the connectors. From this analysis it was estimated that the connectors would begin to yield at approximately 90kN, less than the 190kN required to reach the bending capacity / 245kN required to reach the tensile capacity of the timber joist, and therefore enabling both ductile behaviour and high load capacity.

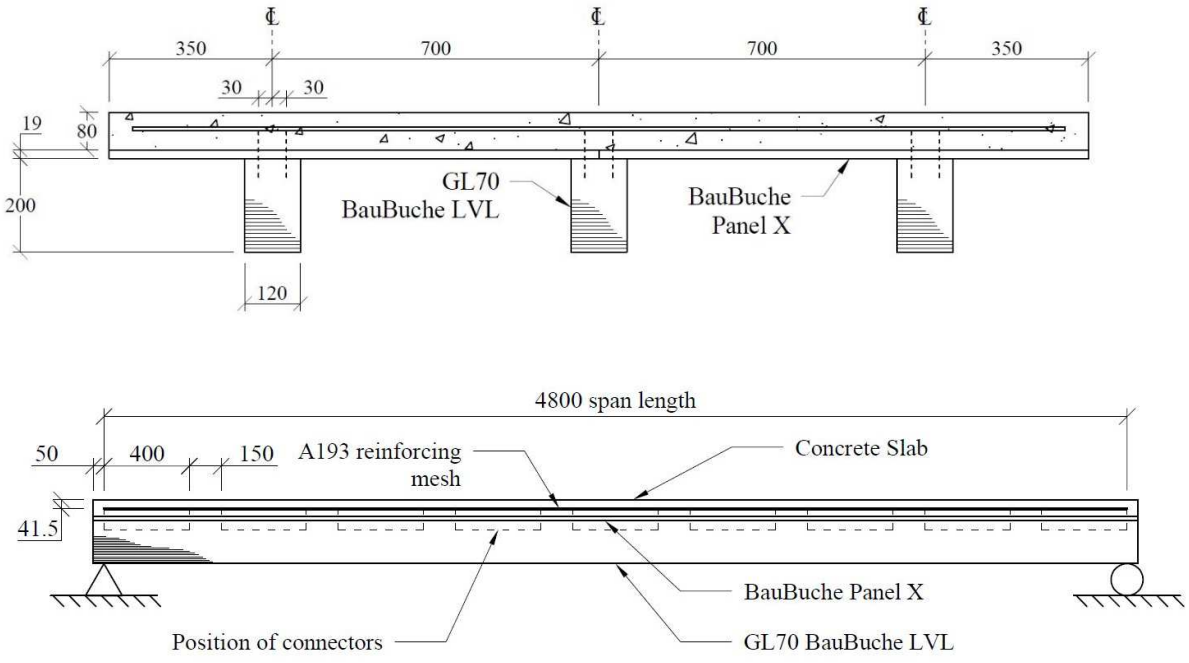


*Figure 5 – (a) Cross-section, and (b) side elevation of full-scale experimental specimen*

Due to space restrictions, this specimen was fabricated in-situ. A temporary formwork was constructed above the LVL joists using the interlayer as a base (Figure 6(a)), into which the concrete was then cast and compacted. The concrete was left to cure for 40 days before testing began. Figure 6(b) shows the freshly cast concrete slab.

*Figure 6 - Formwork for three-joist specimen (a) before concrete pour, and (b) following the concrete pour*

A testing regime was devised which would enable repeat loading of the structure at distinct locations to explore the load sharing capabilities of the specimen, without initially affecting the linear-elastic behaviour of the structure or connectors. This required all loading to be conducted within service level loads to prevent plastic deformation of the structure. A 20kN load was estimated as being appropriate for these uncracked stage explorations. Load was always applied onto the slab, first directly above the middle joist and then directly above one of the off-centre (edge) joists.

The load was applied using a servo-hydraulic actuator, and specimen response was recorded. For the lower concentrated loads within serviceability limits, a 50 x 50mm steel plate on a rubber pad was positioned between the load cell and the surface of the concrete slab, as recommended in Eurocode 1, Section 6.3.1.2(5) [35]. For the load-to-failure test, this was increased to a 200mm x 200mm plate to inhibit local crushing or punching through of the concrete.

Due to limitations of the testing frame, the actuator could only be positioned directly above the centre-line of the specimen and, therefore, could not directly load the slab over the edge joists. Hence a transfer structure was designed to enable loading of the off-centre joists, see Figure 7. The actuator applied load to a transversely oriented I-section, which in turn transferred the load to the edge joist.

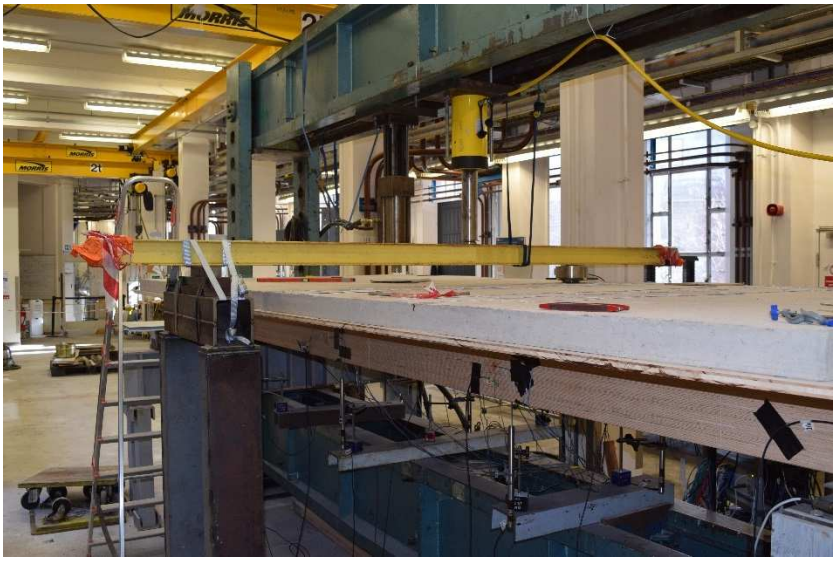

*Figure 7 - Transfer beam structure for off-centre loading*

### 2.2.1 *Instrumentation*

The mechanical behaviour of the specimen was monitored using a comprehensive set of instrumentation shown in Figure 8. As stated earlier a key aim of the research was to determine moment sharing across the specimen, and this was achieved by experimentally deriving a through-depth strain distribution, and subsequently converting those strains through the section to stresses, forces, and then moments. In order to be able to determine these strain distributions, a specific layout of strain gauges was required. The underpinning principles of this layout are as follows:

- Three gauges placed at distinct levels through the depth of timber joist allowed the calculation of curvature in the joist. In practice, as seen in Figure 4, five gauges were used in order to allow for any asymmetry in the joists, by averaging out the two values at each of the upper two gauged levels within the joist section, to get strain values for the centreline of the joist.
- Bi-axial gauges placed on top of the slab, directly above the corresponding gauges on the joists, enabled determination of the longitudinal and traverse strains there, and also investigation of shear lag effects at the top of the slab. The steel rebars of the A193 mesh were of too small diameter and were too smooth (giving rebar-concrete slip) to allow strain recordings that were meaningful in the context of the slab, while the formwork interlayer prevented reliable

placement of gauges at the soffit of the cured slab. Also note that gauges placed through the depth of the slab's exposed vertical edges would have led to strain readings not applicable across the width of the slab.

- The above limitations meant that it was not possible to place gauges at multiple levels through the slab. Consequently, an assumption of full slab-to-joist curvature compatibility was used along with the single longitudinal strain at the top of the slab, to enable determination of the entire through-depth longitudinal strain distribution in the slab. Once the strains had been converted to stresses and ultimately moments, the validity of this curvature compatibility assumption was checked by comparing the sum of the moments in each T-section with those deduced from equilibrium requirements (see Figure 10 and Figure 13).
- The double shear connection test results were used to determine where through the depth of the interlayer that the slip strain should be applied.

All strain gauges were of the electrical resistance type. In order to achieve the above objectives, these gauges were strategically placed at six distinct locations, namely at mid-span and at one quarter-span location of each joist. At each location the timber joist was instrumented with five gauges as described previously, and directly above a 90$^{o}$ bi-axial gauge was placed on the concrete slab's top surface (Figure 4). Four more longitudinally oriented gauges were placed on the top surface of the slab at mid- and quarter-spans, halfway between joists and also at the edges of the slab, in order to better determine the transverse distribution of longitudinal strains (Figure 8).

In addition to this ad-hoc and important strain gauge layout, a load cell was positioned at each support of each joist, six in total, to evaluate the distribution of support reactions across the width of the TCC specimen. An additional load cell was placed beneath the forcing actuator to enable conduct of equilibrium verification checks. Linear variable displacement transducers (LVDTs) were used to measure displacement at quarter- and mid-span locations along the specimen under each joist, and slip measurements were taken using linear potentiometers placed between the timber joists and timber interlayer. Five slip gauges were used per joist, spaced equally along the length, at both ends, mid-span and at quarter-spans. Whilst these types of instrumentation have been used in previous research on

multi-joist TCCs, the focus in these prior studies has been on behaviour in the linear regime, whereas the research reported on in the present paper uses the instrumentation to capture data well into the non-linear regime up to failure.

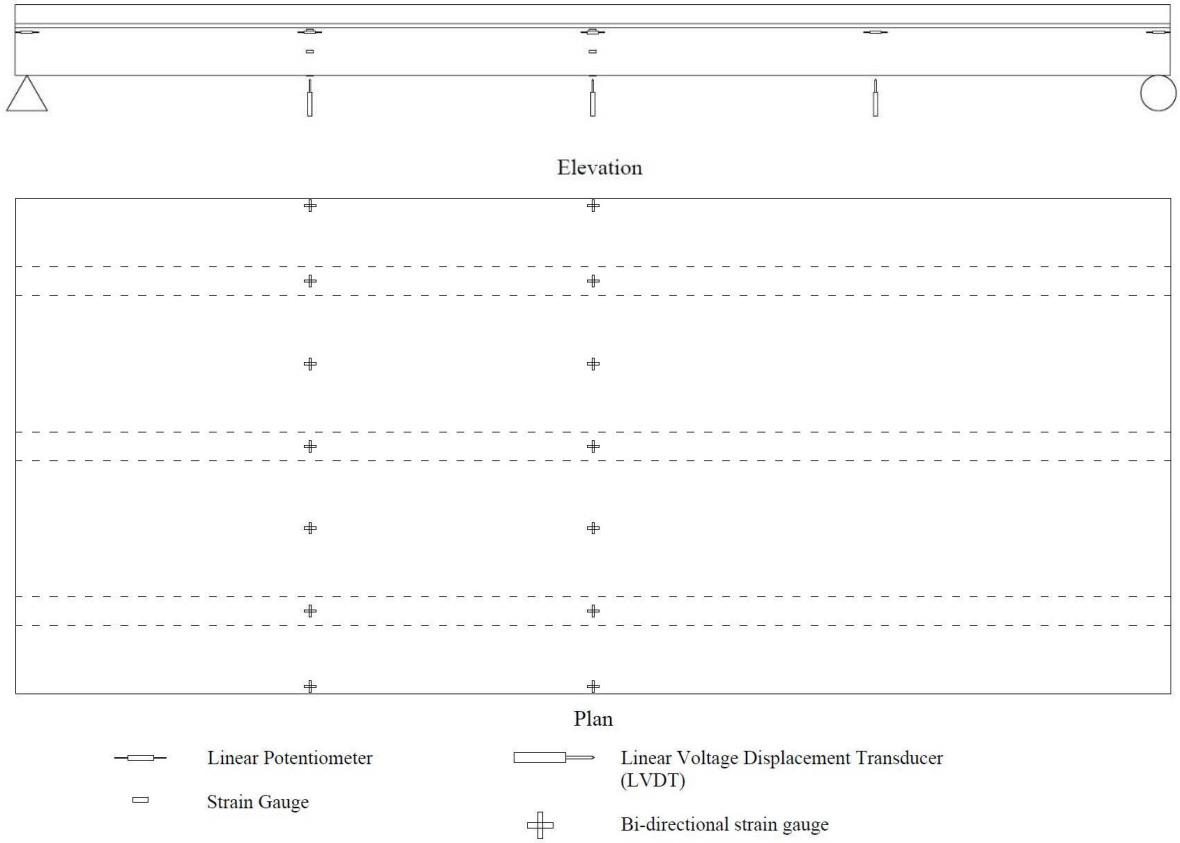


*Figure 8 - Instrumentation used on the specimen (not to scale). Instrumentation on the Elevation is per-joist.*

## 3 Results and Discussion

The following section describes the following:

- The disparity between moment sharing and reaction sharing profiles across the specimen at service loads and up to failure.
- The behaviour of the specimens during the wet concrete loading stage
- Global structural behaviour at service loading and up to failure
- Structural characterisation of the shear connection and further analysis of its behaviour

## 3.1 Load sharing profiles comparison

Throughout the remainder of this paper joists J1, J2 and J3 refer to an edge joist, the middle joist and the other edge joist respectively. Likewise M2M, R1, M3Q, etc refer to the moment at midspan for the T-section including joist J2, to the support reaction for the T-section including joist J1, to the moment at quarter-span for the T-section including joist J3, etc.

To calculate the bending moments in the TCC specimen, the strain gauges that were placed strategically through the depth of the specimen were utilised as part of a Multi-Layer Analysis (MLA) tool developed for this purpose. Figure 9 shows the through-depth strain distributions recorded at mid-span of the TCC T-section including joist J3 for different applied loads. Compressive strains are positive. The markers represent the strains as recorded via the gauges, and the through-depth distributions are obtained as described in Section 2.2.1. The location of slip is assumed to be at the interlayer-joist interface (see Section 3.5.1), and therefore the strain profile is continuous throughout the slab and interlayer, again assuming curvature compatibility between the two components.

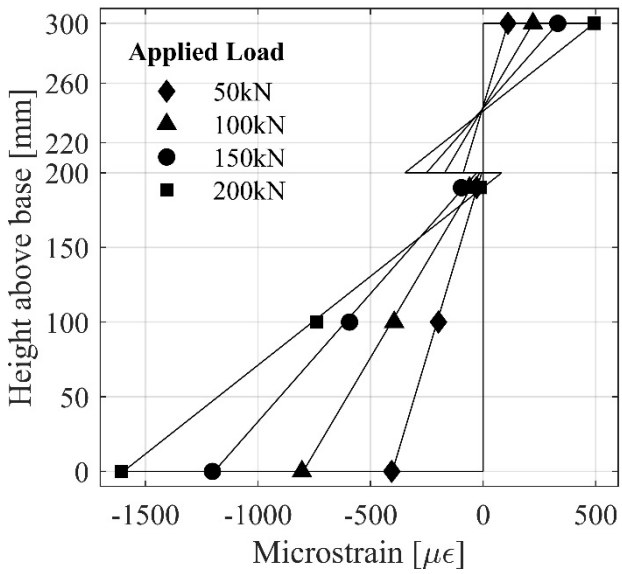


*Figure 9 - Through-depth strain plot for TCC section based on joist J3 at mid-span*

In the MLA approach the cross-section of the specimen was divided into 1mm thick layers. A sensitivity study showed little change in section force for layers of lower thickness. The through-depth strain distribution was then used to apply a strain value to each layer. These layer strains were converted to layer stresses, then layer forces, the values of which and the moments about a fixed point of which were algebraically summed to give the gauged TCC section axial forces and moments respectively. The bending moments were converted into a percentage share per T-section, and then plotted on the same axes as the support reaction share per T-section for comparison. This process was carried out for every load increment during each test, so that moments could be plotted against applied load. The plots also include an "expected value" which was derived from equilibrium requirements.

Three cases were assessed when running these MLA analyses, as follows:

- Case 1: No structural contribution from the timber interlayer, nor from any concrete in tension (concrete cracked for MLA layers in tension).
- Case 2: No structural contribution from the timber interlayer, nor from the concrete only when exceeding the experimental tensile capacity of 3MPa (concrete cracked for MLA layers in tension exceeding 3MPa).
- Case 3: Full structural contribution from the timber interlayer, and from the concrete up to and including the experimental tensile capacity of 3MPa (concrete cracked for MLA layers in tension exceeding 3MPa)).

The first case is a commonly used assumption for finite element modelling, and the third an optimistic assumption of obtaining the maximum structural contribution from the constituent materials, with the second providing an intermediate value.

The presence of the steel reinforcing mesh was not taken into account in the model for the following reasons:

- As seen in Figure 9, and verified for all other analysis cases, the strain at the mid-depth of the slab is in compression, and therefore the additional benefit provided by the reinforcement is minimal in compression concrete.

- The position of the neutral axis remains almost constant during testing, and therefore it is not expected that steel reinforcement at the mid-depth of the slab could be expected to be within cracked concrete before failure.
- The area reinforcement is less than 200mm$^2$ per metre width of slab and so its contribution in any case is minimal.

An assessment of potential tension stiffening of the concrete stab due to the tensile capacity of the underlying timber interlayer was also conducted, but provided no determinable benefit in the results compared to those that are presented in this paper.

### 3.1.1 *Results at service load*

Figure 10 shows bending moment against applied load for the load applied directly on joist J3 at mid-span. The results show a linear trend which follows the expected value closely, deviating at 20kN by 7.9% for case 1, 5% for case 2, and 1.4% for case 3. Therefore, for the results presented for service loads, case 3 will be used in subsequent analysis.

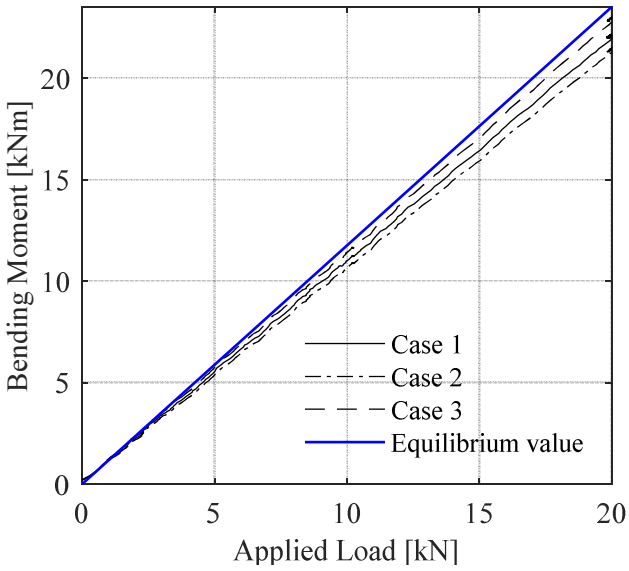


*Figure 10 - Bending moment vs applied load at mid-span for joist J3 loaded up to 20kN*

Figure 11 and Figure 12 compare the support reaction and midspan moment shares for the T-beam corresponding to each joist, as calculated using the MLA. In Figure 11, the support reaction and moment share for the crucial T-beam of the directly loaded joist J2 are similar, to within 4% of each other

between 3 and 20kN, indicating that use of the two values interchangeably would be appropriate for design of this joist under this specific external load. However Figure 12 shows that when one of the outer joists is loaded there is a distinct difference between support reaction sharing and moment sharing. Indeed it is seen that in this situation, the bending moment share for the T-beam of joist J3 is about 15% less than that of the support reaction. Otherwise note that the results show a distinctly linear response to load (after a small period of the structure settling). This suggests that at service loads the structure experiences little nonlinearity in either support reaction or moment distributions, an important consideration for SLS design.

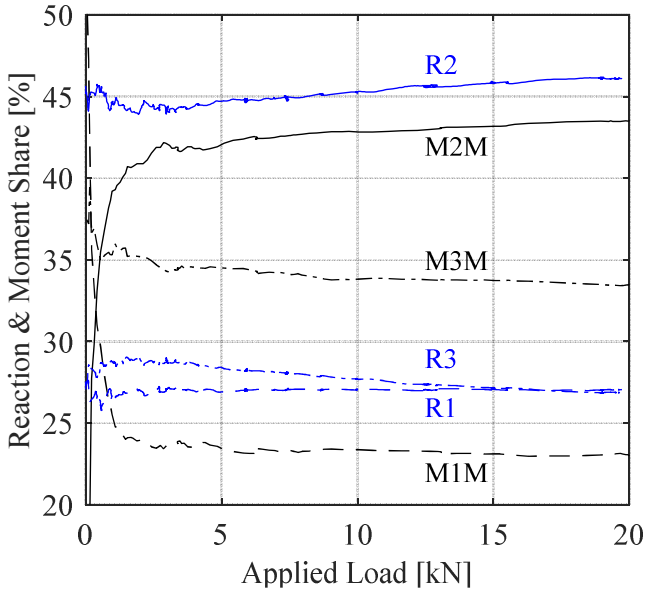


*Figure 11 - Comparison of support reaction and mid-span moment share for joist J2 loaded at 20kN. R(X) signals summed support **R**eaction of joist **X**, M(X)M signals bending **M**oment share of joist **X** at **M**id-span.*

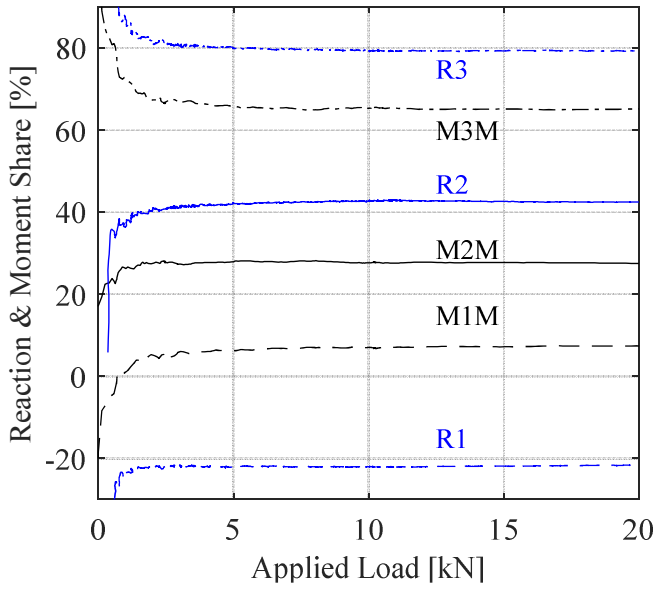


*Figure 12 - Comparison of support reaction and mid-span moment share for joist J3 loaded at 20kN. R(X) signals summed support **R**eaction of joist **X**, M(X)M signals bending **M**oment share of joist **X** at **M**id-span.*

### 3.1.2 *Failure load test data reliability checks and moment sharing assessment*

Figure 13 shows the three sets of equilibrium checks made on the specimen based on the failure test data. Key comments are as follows, namely:

- Figure 13(a) shows that the support reactions summed up almost to the applied load throughout the test, giving confidence in the load cell readings which underpin this plot.
- Figure 13(b) shows that, up to quite high applied loading, the slab section axial force at midspan very nearly equates to the summed axial forces from the three joists at the same gauged section. All of these axial forces have been obtained via the MLA approach and so are based directly on the recorded midspan strains. This relationship between the slab and joist axial forces is almost fully consistent with the longitudinal equilibrium requirement, an observation which vouches for the high quality of the recorded strain data.
- In Figure 13(c) the bending moments obtained via the MLA method, using each of the three cases set out in section 3.1, and also the moment required by equilibrium, are all plotted against

applied load. The results show that all three MLA cases follow the equilibrium curve closely up to well beyond the onset of non-linearity. Indeed for cases 1 and 2 the comparisons against equilibrium are very good up to the 200kN peak load achieved in the tests.

These above three sets of comparisons gave quite high confidence in the recorded load and strain test data for assessing support reaction sharing and moment sharing. These are now discussed.

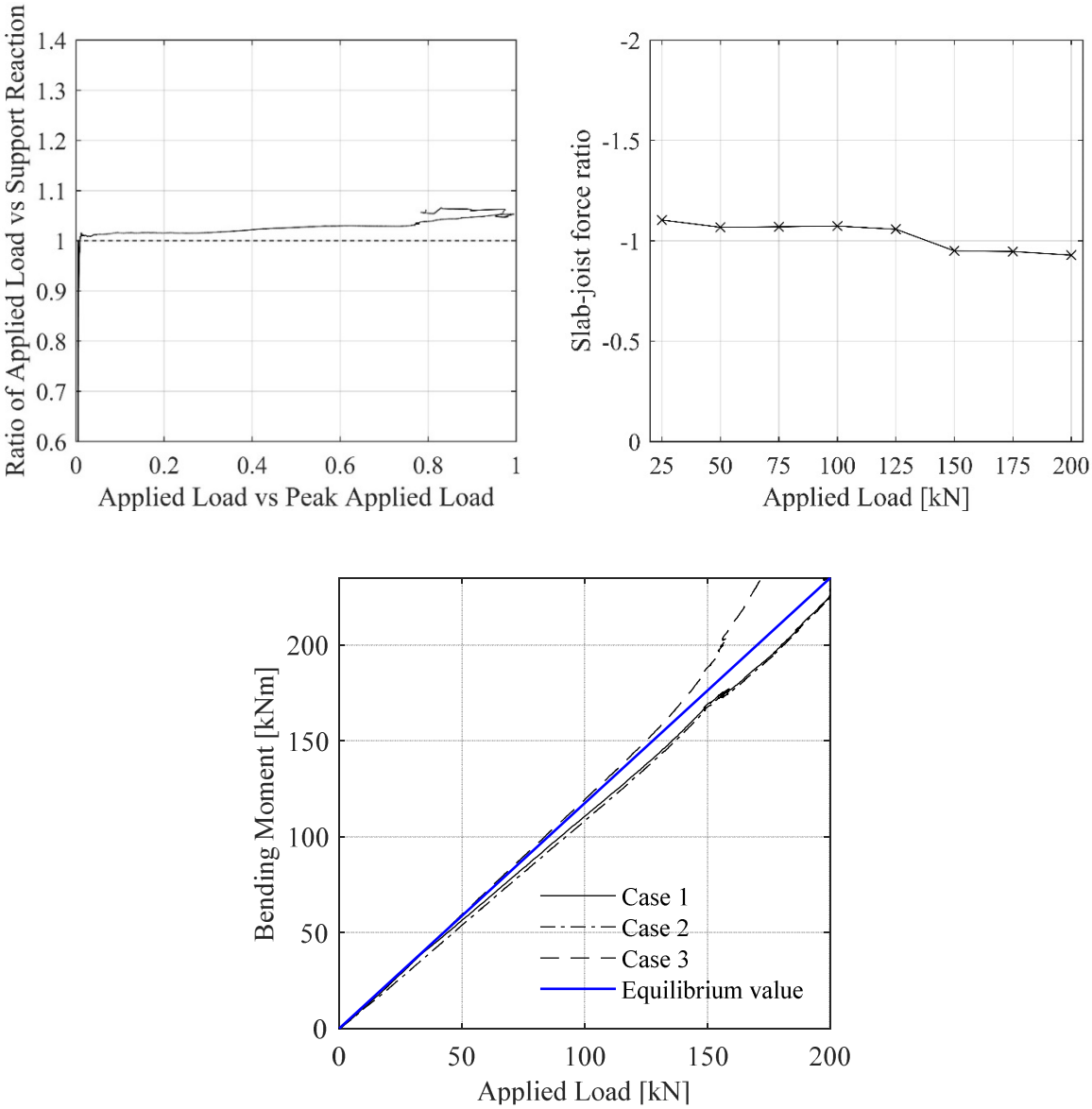


*Figure 13 – Equilibrium verification for Failure Test Data: (a) Reactions Relative to Applied Load, (b) Slab section axial force relative to section axial force from joists combined, (c) Midspan moments*

Figure 14 and Figure 15 show the relationship between support reaction share and bending moment share at mid- and quarter- spans respectively. It is seen that the share of the maximum support reaction, R2, varied considerably throughout the test, indeed increasing by a peak of 23% during the test. At midspan (Figure 14), the maximum moment share M2M shows three distinct regimes, namely nonlinear between 0kN and 40kN (which contrasts with the largely constant moment sharing seen during the earlier 20kN test maybe due to changes in the specimen from repeated load tests), followed by constant moment share between 40kN and 150kN, and finally rapidly changing moment share M2 in the approach to failure. It is seen that the support reaction share exceeded both the mid- and quarter-span moment shares. For the largest (i.e. J2) midspan moment the difference between the two sets of sharing profiles peaked at about 18% at midspan (49% moment vs 67% reaction at 150 kN applied load) and a highly significant 29% at quarter-span. This shows that design of a TCC floor based on a moment distribution that mimics the support reaction distribution could lead to quite a conservative design.

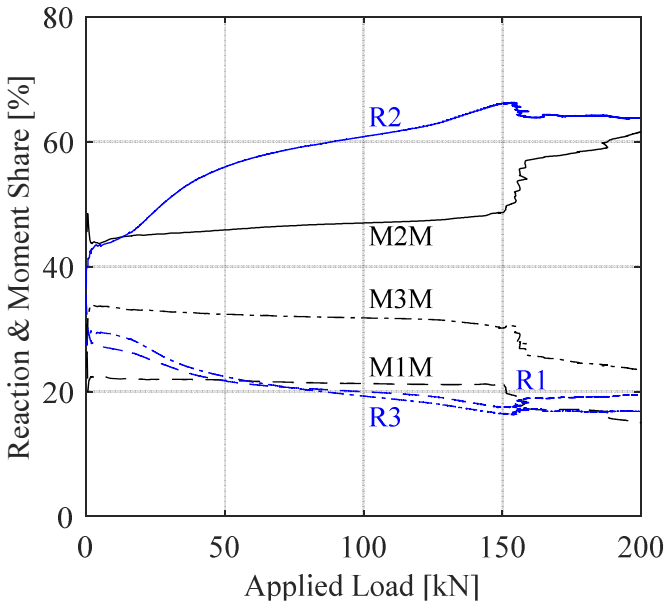


*Figure 14 - Comparison of support reaction and mid-span moment share for joist J2 loaded at 200kN. R(X) signals summed support **R**eaction of joist **X**, M(X)M signals bending **M**oment share of joist **X** at **M**id-span.*

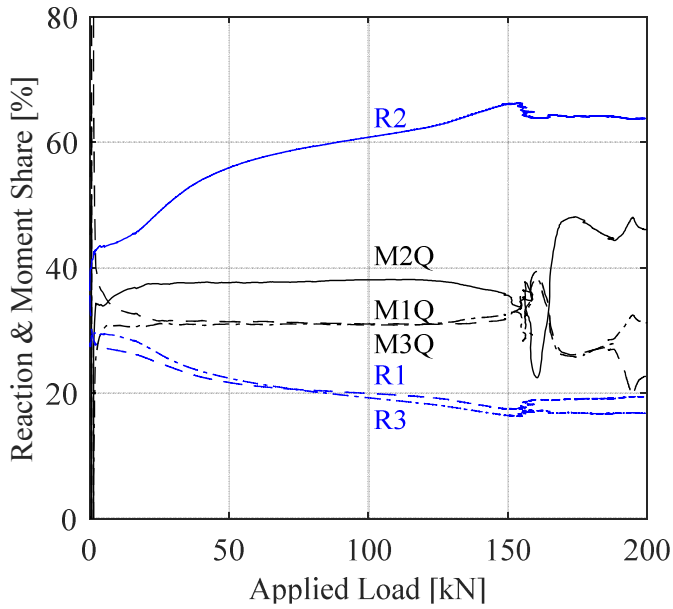


344

345 *Figure 15 - Comparison of support reaction and quarter-span moment share for joist J2 loaded at 200kN. R(X) signals*
346 *summed support **R**eaction of joist **X**, M(X)Q signals bending **M**oment share of joist **X** at **Q**uarter-span.*

347

348

349

## 3.2 Wet concrete stage moment sharing

Mid-span deflection and soffit strain variations with time, as recorded from each joist during the concrete cast, are presented in Figure 16. The steps on both sets of plots are due to repetition of pouring then spreading of concrete onto the formwork interlayer. Each plateau corresponds to the pause between the previous batch of concrete having just been spread and the arrival of the new batch. It is seen that the strains at the conclusion of casting reached up to 210 με, broadly similar to the strains experienced under the low-level concentrated load test discussed in Section 3.3, and approximately 4% of the strains achieved at peak load during the failure test on the specimen discussed in Section 3.3. This shows that in comparison to service level loading, the strains induced by the casting and subsequent curing of the concrete are significant and should be considered, however they become of less importance when ULS design is considered.

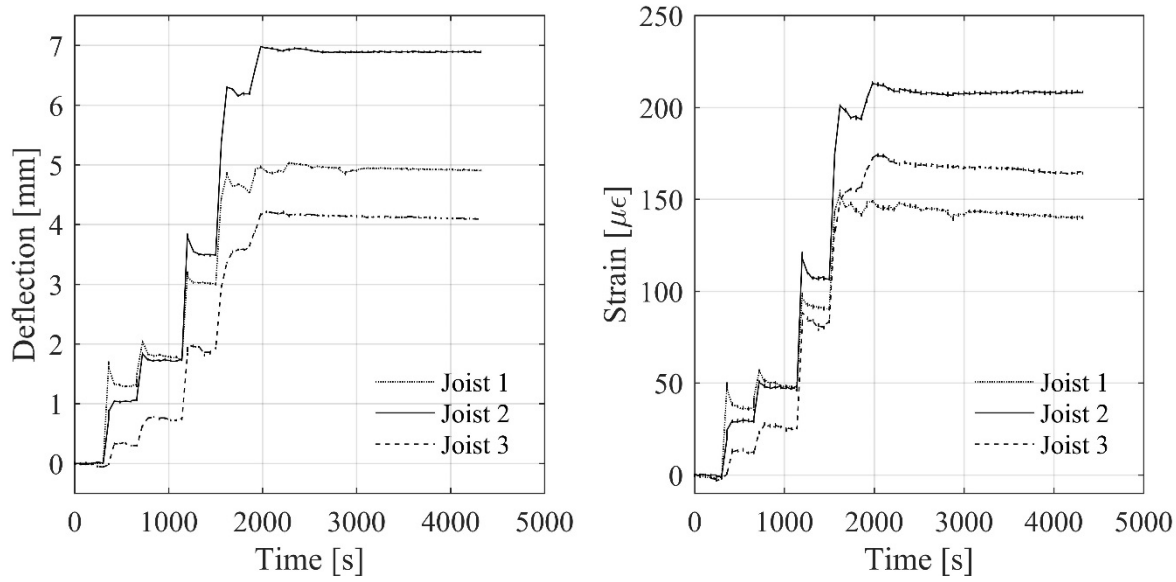


*Figure 16 - (a) Deflection of joists mid-span, (b) joist soffit mid-span strains, during casting of the concrete slab*

Let us now assume that the timber structure at this wet concrete stage acted as three adjacent T-sections in longitudinal bending, where each T-section comprised one joist in full composite action with the overhead interlayer of width halfway between the joist in question and its nearest neighbour(s). If the section flexural stiffness (*EI*) value calculated for this section is combined with the midspan strains recorded at completion of casting, it is found that the outer and middle T-sections carried midspan moments due to wet concrete loading of 3.14 kNm, 3.7 kNm and 4.64 kNm respectively. This equates

to 27%, 32% and 41% moment sharing at midspan, not too dis-similar from the ratios seen at the composite-stage when a midspan concentrated load was applied directly above the middle joist, see Section 3.4. Note also that the sum of these three T-section moments equates to 11.4kNm, which closely approximates the 12kNm value required for equilibrium. This vouches for the high quality of the recorded strain data at the wet concrete stage.

## 3.3 Composite Stage – Other facets of global structural behaviour up to ultimate load

During the failure test the specimen was subjected to gradually increasing load first up to 100kN, then up to 125kN, with a period of slow unloading after each, followed by a final loading to failure.

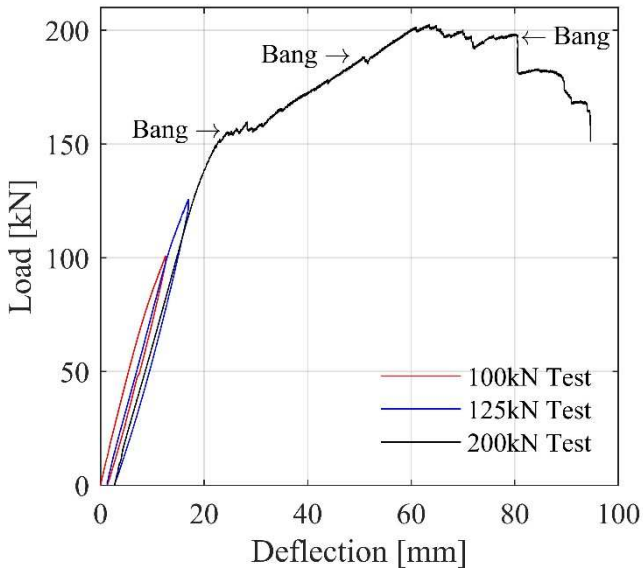


*Figure 17 - Load vs deflection of TCC specimen*

Figure 17 shows the corresponding load-deflection plots. It is seen that the specimen exhibited similar responses to the repeated load cycles. Following each test there was some deflection (1.4mm and 1.3mm respectively) that was not fully recovered, and therefore on each subsequent reloading cycle the specimen moved along a slightly different trajectory. Figure 17 shows multiple and distinct stages of behaviour, as follows:

- High-stiffness, linear load response up to just over 150kN;
- A drop to almost zero tangent stiffness over a short (approximately 8mm) range of deflections;
- A sharp rise in stiffness, akin to strain hardening, and of constant gradient up to peak load;

- A subsequent holding of the load at the roughly constant peak value, resembling ductile behaviour, over a 20mm (60 – 80mm) range of deflections;
- Load drop to failure by (Figure 18) splitting of the slab at the support connectors, midspan flexural fracture of J2, plus J2-aligned and oval cracks (traced in Figure 18(c)) in the slab.

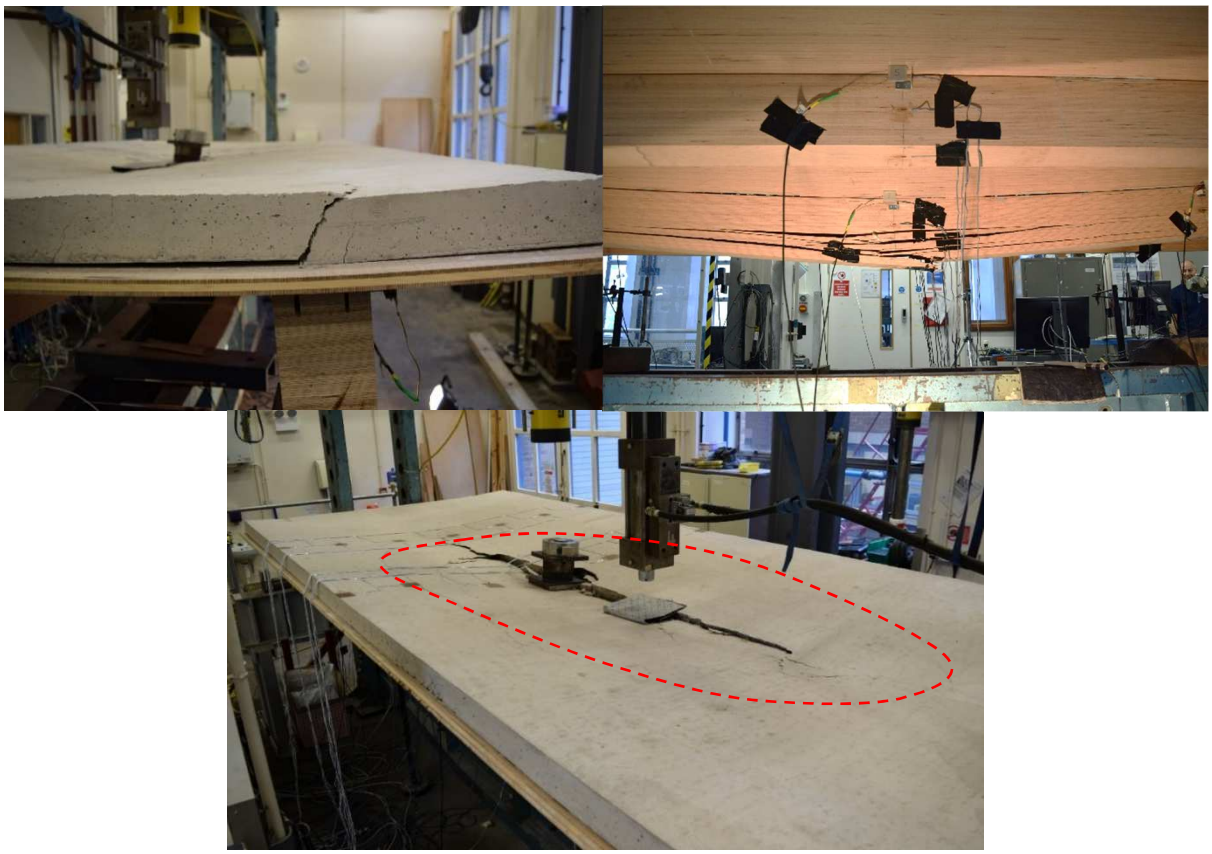

*Figure 18 - TCC Specimen Failure Modes – (a) Slab end split, (b) Fracture of J2, (c) Oval cracks and major split*

The slab itself deformed in a bowl-like manner (which might have created membrane effects that in turn induced the oval crack of Figure 18(c)), with significant deflection at its centre under the

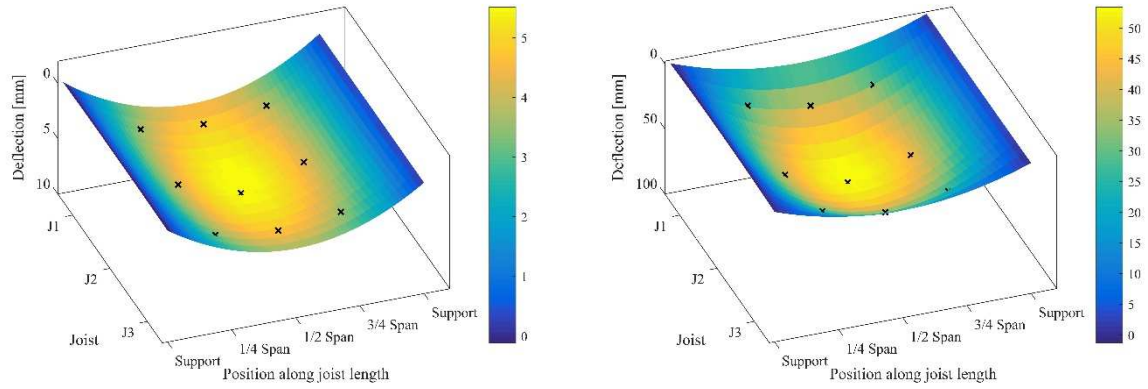


*Figure 19 - Interpolated deflection profiles of the specimen at (a) 50kN and (b) 200kN. X's mark locations of measurement.*

concentrated loading. This contrasts with the lower loads, where the bowl effect was not as pronounced, as shown in Figure 19.

During the short regime of sharp drop in stiffness (Figure 17) which started just above 150kN, oil had to be supplied at an increased rate to the piston of the loading jack, to continue increasing specimen deflections. It is seen that many of the kinks in the plot of Figure 17 were accompanied during the test by loud bangs, which signalled the above and other possible local failures in the timber interlayer and concrete slab.

Figure 20 shows the load redistribution which occurred, as the test progressed, from the outer joists (J1, J3) to the central joist (J2), with the total reaction share of the two outer joists reducing monotonically from over 50% at low loads, to 34% at the point of nonlinearity, indicating the decreasing ability of this TCC structure to distribute load transversely between its adjoining T-sections, and highlighting the nonlinearity of the support reaction sharing with increasing load.

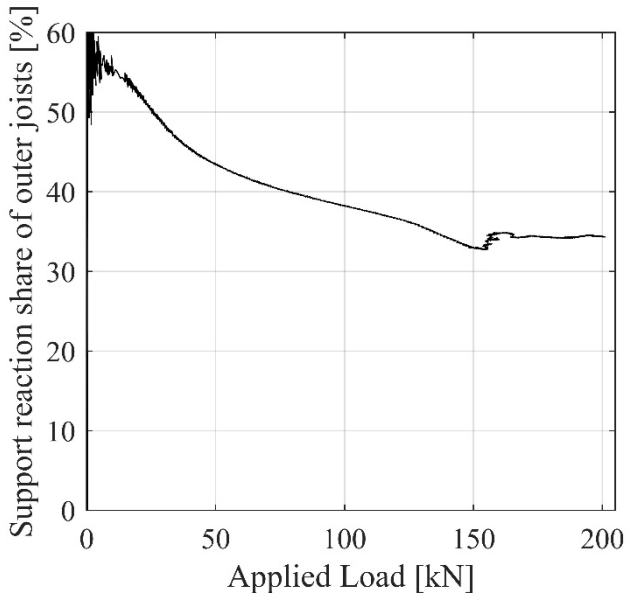


*Figure 20 - Load redistribution from outer joists to central joist*

Figure 21(a) shows the increasing support reaction with load for the six supports. The trend is generally linear, although there is some notable nonlinearity at low and high loads. A small degree of specimen asymmetry can be seen here as shown by the divergence in support reaction between near- and far-supports of the same joist, especially for joist J2. Nevertheless, the general trend is as expected with the

central joist J2 taking an increasingly larger proportion of the total load. At 155kN there is a noticeable discontinuity, which correlates with Figure 17. The support reactions after this point again increase linearly but at a different gradient, as suggested by the corresponding deflections. This occurrence is contemporaneous with the observation of vertical splitting at the connections in the end zones of the slab as shown in Figure 18(a) and discussed above.

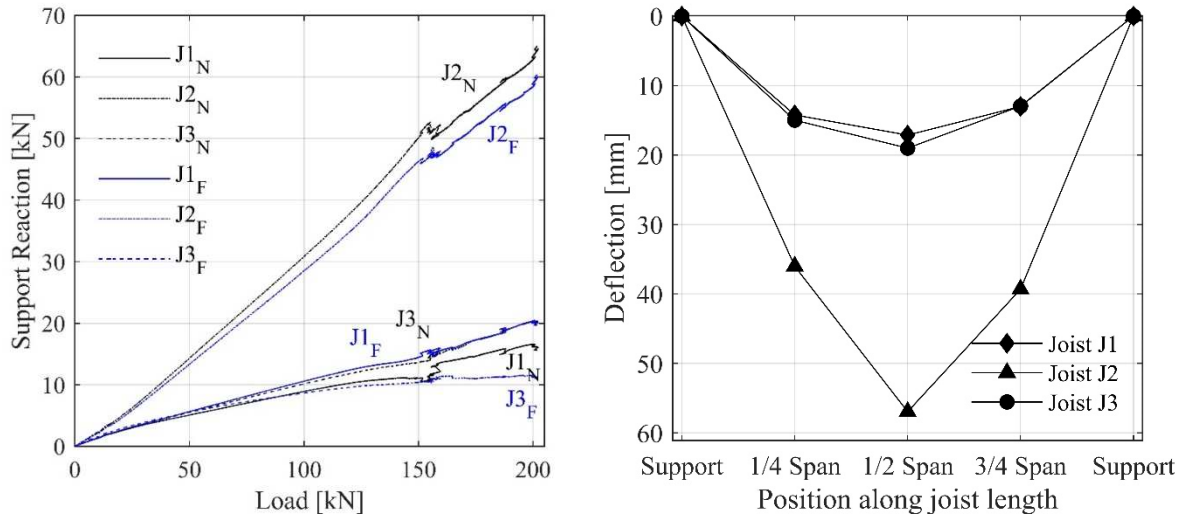


*Figure 21 - (a) Support reaction profiles vs total applied load, (b) Deflection profiles at 200kN*

The deflection profiles of all joists are shown in Figure 21(b). The clear dominance of the J2 profile over the J1, J3 profiles further reinforces the point that a quite high fraction of the applied load was borne by the J2 T-section in relation to the outer T's. At 200kN the load and deflection sharing profiles are quite similar to each other, with the central joist taking 64% of the support reactions and 61% of the deflections, with similar shares of around 18% each for the outer joists for both support reaction and deflection.

### 3.3.1 *Post-test visual observation of connections*

Cutting of the specimen into pieces to facilitate disposal enabled confirmation that the oval and longitudinal cracks shown in Figure 18(c) had propagated through the full-depth of the concrete slab. Exposing the connectors by excavating out the concrete slab showed that these connectors remained intact post-failure of the overall TCC specimen.

As Figure 22(a) shows, the midspan zone connections did not experience pull-out failure from the joists as may have been initially thought due to some of the loud bangs heard during testing. Of course,

connector-to-slab failure cannot be ruled out. The connectors at the extremities of joist J2 were also still firmly embedded within the timber after the test (Figure 22(b)) and showed no signs of deterioration at the concrete-interlayer interface. The same is true for the connectors along J1 and J3, which also showed no signs of deformation above or below the timber interlayer. Hence the splits in the slab above the joist, observed in the support zones as shown in Figure 18(a), might not have led to plastic deformation of the raised steel mesh connectors.

*Figure 22 - Post-test observation of (a) central connector on joist J2, and (b) end connector on joist J2.*

## 3.4 Structural action under other load layouts in the elastic regime

Recall that before the specimen was loaded to failure, it was also tested within the linear elastic loading regime, by applying a concentrated pad load of up to 20kN to the slab directly above the centreline of each joist at mid-span. The transverse load sharing properties of this structure can be seen when comparing the deflections of the edge- and centrally-loaded joists, see Figure 23. Maximum deflection (at mid-span) of the edge-loaded tests reached 3.6mm for J1 and 3.5mm for J3, reducing to 0.2mm at each opposite edge-joist. The central joist deflected only 1.9mm when placed under the same 20kN load, decreasing to 1.5 and 1.6mm in the adjacent joists. The distribution capabilities of the specimen are clearly seen here, although a non-symmetry is highlighted by the difference in resultant deflections of the edge joists. This is due to inherent imperfections which arise in constructing such large specimens and needs to be considered throughout the design process.

Of further interest is the deflection at supports. Whilst no instrumentation was placed at the supports, an extrapolation of the recorded data shows that, for the edge-loaded tests, the joist furthest from the

load exhibited negative deflection, i.e. uplift, of up to 1mm. This is shown graphically in Figure 23 for the test loading joist J1 at 20kN.

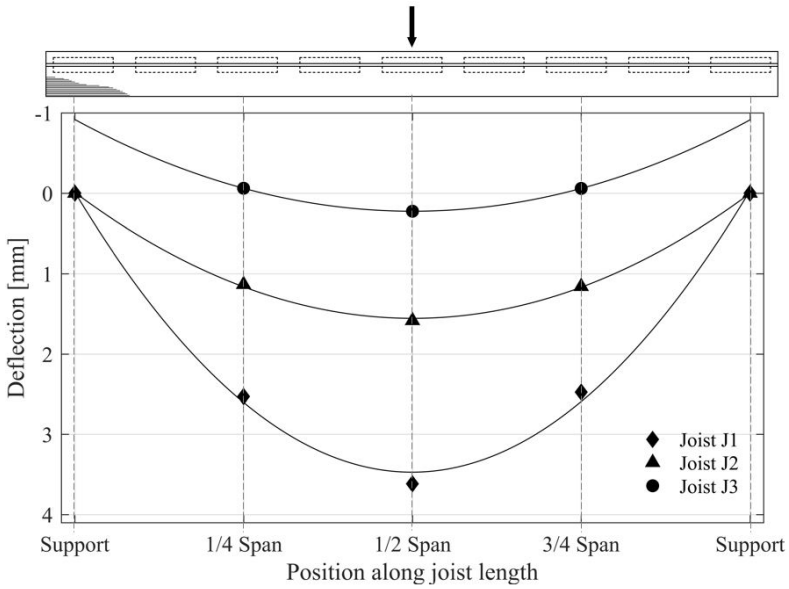


*Figure 23 - Interpolated deflection profiles of each joist for the 20kN test loaded at mid-span on joist J1*

The support reaction distributions for these elastic regime load tests again suggest good transverse sharing capabilities. When the central joist was loaded, the central supports took 44% of the load. However with only one edge joist loaded the corresponding edge supports carried 80% of the load, with 40% taken by the central supports and -20% taken by the far edge supports, representing an uplift force on that far edge and reaffirming the extrapolation of deflection data to assume an uplift of the slab. Small uplifts were able to be recorded, by zeroing the load cells with the specimen resting on them: therefore, any reduction in load (i.e. uplift) up to the level of the unloaded specimen was able to be noted. This uplift at low loads emphasises the excellent transverse stiffness of the slab, which allowed it to distribute load when joist J2 was loaded, and in this situation, to have supported the uplift of the slab. There is good consistency between support reaction totals for each end of the specimen, with the far end taking 48% and 44% for the central- and edge- loaded tests respectively.

Figure 24 shows the summed support reactions for each of the three service-level load cases. These profiles more closely approximate a symmetrical distribution than do their deflection counterparts. Note

463 that these support reaction sharing profiles do not mimic the highly nonlinear bending moment sharing
464 profiles as presented earlier in this paper. It is thus worth reiterating that provision of these experimental
465 moment sharing profiles is a novel feature of this study.

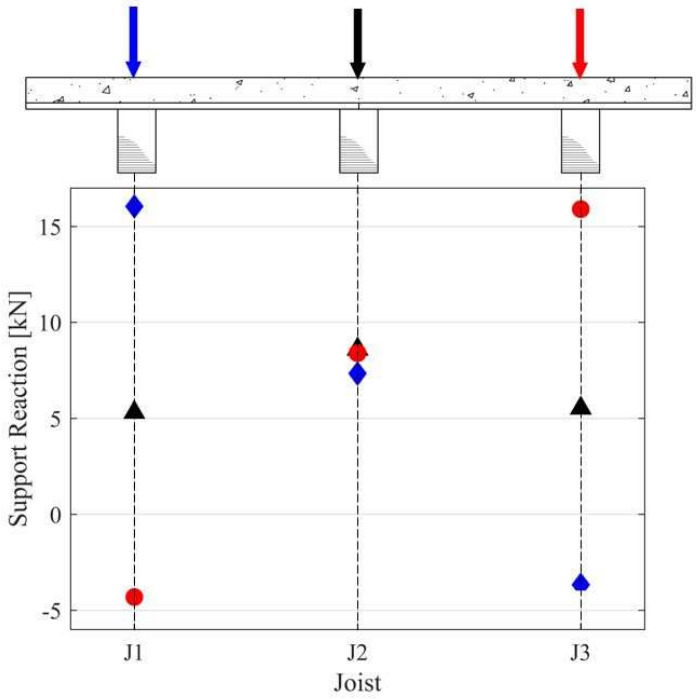


466

467 *Figure 24 - Summed support reaction profiles for each of the 20kN low-load tests*
468

469 Profiles of transverse strain (tensile positive) for the top of the slab at midspan are given in Figure 25
470 for all three loads. The lower quarter-span readings are omitted. It is seen that the largest compressive
471 strain (236 με, due to transverse negative bending) occurred when load was above J2.

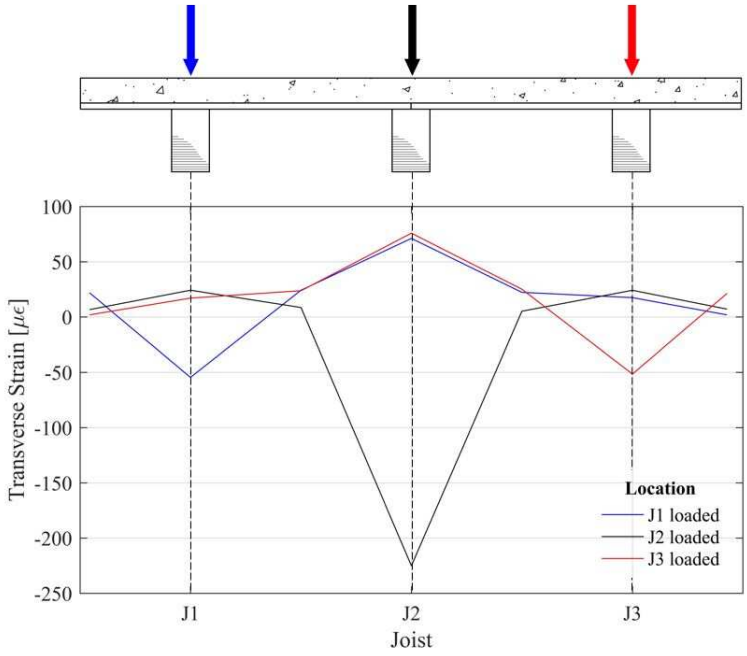


*Figure 25 - Concrete transverse strain profiles at mid -span for the three low-level 20kN load cases.*

Loading the edge joists led to lower peak transverse compressive strain (above the loaded joist) than did loading the central joist, but it did lead to higher peak transverse tensile strain (above the adjacent joist) than did loading J2. At quarter-span no transverse tensile strain was recorded in either edge-loaded case. Comparing the longitudinal and transverse strains for loading above joist J1, the longitudinal strains were lower in absolute magnitude at quarter-span, and higher at mid-span. In addition, at all four locations away from the loaded joist, the recorded transverse strains indicated negative transverse moments whereas the recorded longitudinal strains indicated positive longitudinal moments. Table 1 shows the ratios of longitudinal-to-transverse strains at these locations.

*Table 1 - Ratio of longitudinal to transverse strains for 20kN loading above joist J1*

| Span location | Ratio of strains | | |
|---|---|---|---|
| | J1 | J2 | J3 |
| Quarter-span | 0 | -0.7 | -0.8 |
| Mid-Span | 0.4 | -1.6 | -1.2 |

These results suggest that in the linear elastic regime the concrete slab provided good transverse stiffness to enable effective load sharing between adjacent joists. This load sharing was most

pronounced in situations where the loaded joist could distribute load in two directions. At these loads the transverse strains in the concrete were not significant.

## 3.5 Shear Connection Behaviour

### 3.5.1 *Double Shear test results*

Results of the double shear tests (as defined in Section 2.1) conducted on each of the four connection specimens are shown in Figure 26. The figure shows average load-slip curves for each specimen, taking all four displacement measurements into account.

The average slip stiffness is 505.4 kN/mm across the four experimental specimens, which is an extremely high value. Individual slip stiffnesses ($k_{s,}$ = 0,4 $F_{est}/v_{i,mod}$) and maximum loads ($F_{max}$) are shown in Table 2, calculated using equations defined in BS EN 26891 [37]. The bulges in the initial linear portions of the curves – representing the unload-reload cycles as required by the standard – are small, indicating a low impact of small numbers of load cycles within the early elastic regime.

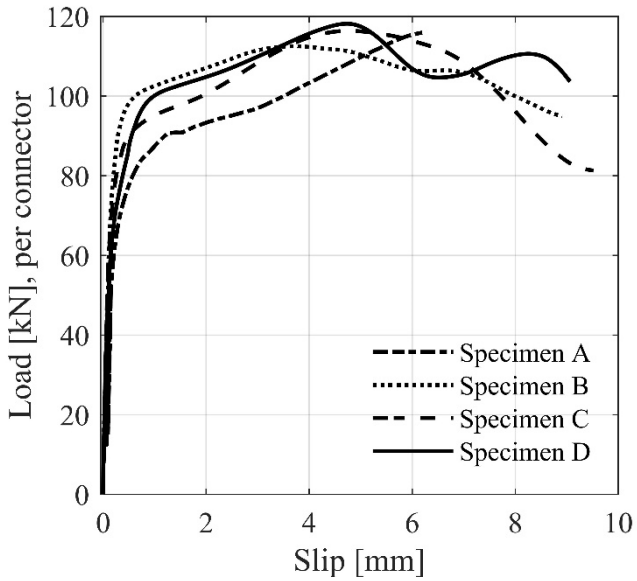


*Figure 26 - Average load-slip curves for the four specimens*

*Table 2 - Load and stiffness properties of double-shear connection specimens*

| Specimen | Maximum load ($F_{max}$) (kN) | Failure mode | Slip stiffness ($k_s$) (kN/mm) |
|---|---|---|---|
| A | 116.3 | Shear rupture of mesh | 406.7 |
| B | 112.6 | Shear rupture of mesh | 614.4 |
| C | 116.5 | Shear rupture of mesh | 581.4 |
| D | 118.4 | Shear rupture of mesh | 418.9 |
| Average: | 115.9 | | 505.4 |
| Coef. of Variation | 0.021 | | 0.213 |

Figure 26 suggests that the connectors also showed good ductility, characterised by a long plateau of minimum approximately 8mm slip. The potentiometers used in the experiment recorded up to a limit of 10mm slip. However, visual observation of markings placed on the joist and slab indicated that slip increased up to at least 15mm for each test before final ductile failure of the connection occurred.

For each specimen, there was plastic failure of the connector, at the interface between the *timber joist and the timber interlayer*. This highlighted the location where the slip-strain should be determined in through-depth strain plots in Section 3.1, and also where to mount linear potentiometers on the full-scale specimens so as to record slip between the joist and slab.

*Figure 27 - Failure planes of the connectors in Specimen A at (a) the surface of the timber joist, and (b) the timber interlayer.*

512 The specimens displayed significant shearing deformation of the connectors before failure. Figure 27(a)
513 shows residual evidence of clear deformation of the connector, which remained well-embedded within
514 the timber joist, whilst Figure 27(b) shows the corresponding remainder of the connector embedded
515 into the concrete via the interlayer. The level of deformation of each connector before failure was high,
516 evidencing the excellent ductility that was exhibited by Figure 26. Following the test, most slab and
517 interlayer portions detached without force - the connector having completely sheared. In other cases,
518 the majority of the connector had failed, but was still connected at discrete locations.

519 ### 3.5.2 *Connection behaviour in full-scale tests*

520 During the elastic regime tests, slip between the slab and joist was negligible. This was deliberate, so
521 as to allow for multiple tests without affecting the structural properties of the specimen. However, at
522 higher loads in the failure test, the slips become much more pronounced, especially in joist J2 above
523 which the load was applied. Figure 28(a) shows the values of slip along each joist at 200kN, as measured
524 by the linear potentiometers. Figure 28(b) shows the slip profile for the central joist J2 with increasing
525 load up to 200kN.

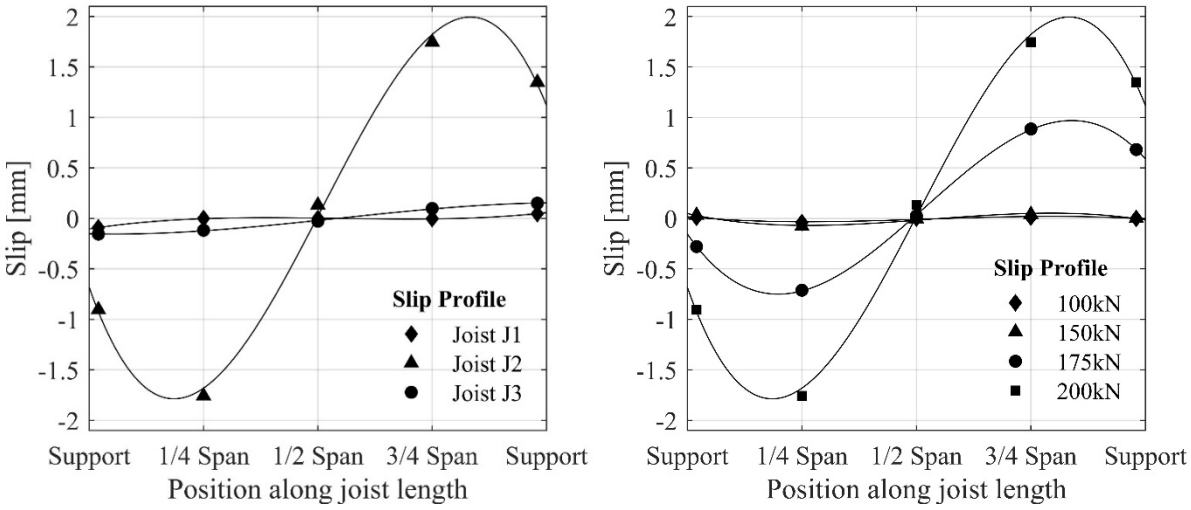


*Figure 28 - (a) Slip gauge readings and interpolated slip profile at 200kN, and (b) interpolated slip profiles for J2 under increasing loads.*

526 These slip profiles were used to determine the slip values at the centre of each of the nine shear
527 connectors along each joist. These slip values were then referenced back to the average connection
528 characteristic from Figure 26, to derive a longitudinal shear force value in each connector. It might be
529 expected that the slip, and corresponding force, were maximum at the extremes of the specimen, but as

seen in Figure 28and this was clearly not the case. At applied loads exceeding 150 kN, this was probably influenced by the splitting of the slab at the end-of-span connections as shown in Figure 18(a) and described earlier. This splitting might well have compromised the abilities of these end connections to transfer load.

In Figure 29(a) the full range of applied load vs connector slip is shown for the two most heavily loaded connectors, 2 and 8, along the J2 T-section. On these plots the sign of the longitudinal slip is deliberately kept the same (despite the reversal which occurred in practice) as midspan is crossed, so as to facilitate comparison between these connection forces on both sides of midspan. Figure 29(b) shows, for each of three different applied load levels, the corresponding forces that relate to the level of slip experienced by each connector. It is unclear to what extent the slab cracks developed in the concrete significantly above 150kN, and thus the plots are only shown up to 155kN, where there is confidence of a relationship between slip and connector force.

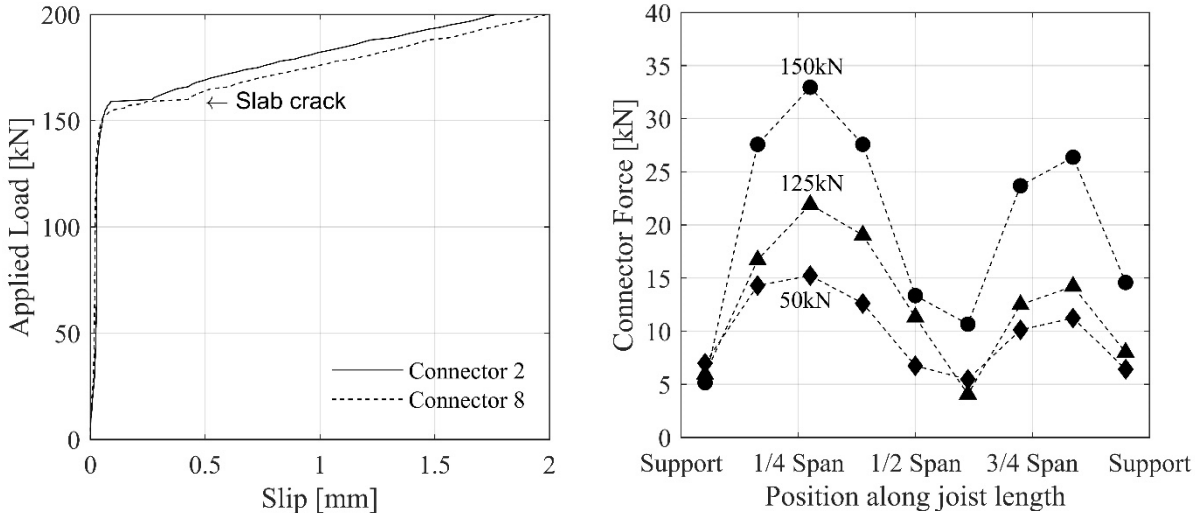


*Figure 29 - (a) Applied load vs connector slip for connector 2 and connector 8, and (b) Connector forces in joist J2 for loads of 50kN, 125kN, and 150kN.*

After reaching peak load on the TCC specimen, the connectors continued to deform. Records from the linear potentiometers highlight that slip at the ends of the specimen between the concrete and timber joist reached up to 7.8mm before the timber fracture occurred, highlighting the excellent ductility of the specimen post-yield, agreeing well with the short ductility plateau following peak load in Figure 17.

## 3.6 Material Tests

Instrumented tensile tests on the timber used in the project led to an Elastic Modulus value of 18.3GPa, higher than that of the manufacturer-quoted value of 16.7GPa. The results of the concrete cube tests are presented in Table 3

*Table 3 - Concrete material properties*

| Concrete Pour | Average Cube Strength ($N/mm^2$) | Std. Dev. | Average Split Cylinder Strength ($N/mm^2$) | Std. Dev. |
|---|---|---|---|---|
| Connector Specimens 1 | 52.4 | 5.6 | 4.2 | 0.29 |
| Connector Specimens 2 | 53.3 | 3.9 | 4.2 | 0.57 |
| Full-scale specimen | 43.3 | 1.1 | 3.3 | 0.12 |

# 4 Conclusions

This paper presents experimental findings of a near full-scale multi-joist timber-concrete composite floor specimen, fabricated from RC32/40 concrete and GL70 hardwood LVL joists, connected by expanded steel mesh shear connectors.

The specimen was comprehensively instrumented to enable recording of support reactions, displacements, timber-concrete slip and strains. The strains were used to calculate TCC section bending moments through the use of a multi-layer-analysis (MLA) model. Before the failure test was conducted on the specimen, elastic regime load tests under concentrated loads were applied at mid-span above each joist to infer the transverse load sharing capabilities of the specimen. Following these elastic regime tests, the specimen was loaded to failure under a concentrated load on the slab above the middle joist, which led to failure at 202kN.

From the work presented in this paper, there are four key novelties that have emerged, as follows:

- The transverse distribution of support reactions and of ¼-span or midspan bending moments can differ significantly from each other in multi-joist timber-concrete composite floors. For the TCC specimen fabricated and tested to failure in this study, the highest share of support reaction was found to have significantly exceeded that of the highest bending moment in the critical joist (67%

vs 49% at 150kN). If taken into consideration, this actual level of moment sharing can enable increased design efficiency when compared to the alternative of basing moment sharing on support reaction sharing. In tests, it is not sufficient purely to measure support reaction distribution in order to understand the midspan moment distribution requirements for the design of TCC floors.

- Whilst within the elastic regime the support reaction and midspan moment shares were each largely constant (but different from each other) with increasing load, the support reaction shares showed increasing nonlinearity at higher loads, whilst the moment distributions remained relatively constant but gave way to sharp nonlinear changes in the close approach to failure.
- A highly effective means of checking the recorded strain data's reliability entails application of curvature compatibility to these data, followed by conversion of the resulting through-depth strain distributions into layered axial forces and then into layered moments both of which have been shown overall to satisfy global equilibrium requirements when algebraically summed. Very importantly, the overall TCC section moments obtained via summation of the layer contributions enabled test data-based quantification of transverse moment sharing.
- The 400 mm long expanded steel mesh plate is highly suited to the role of shear connector in timber-concrete composite floors. Its high slip stiffness and strength (average 505.4kN/mm and 115.9kN respectively), combined with good ductility post-yield meant that it performed well under loading on the present test specimen up to failure.
- The timber-concrete composite flooring using this connection method, and in the layout presented in this paper, failed primarily due to fracture of the timber in the zone of peak moment directly under the applied load (for a simply-supported arrangement), following significant plastic deformation of the specific connections tested in this study.
- It is recommended that any future computational modelling of TCCs use a model of the complete structure rather than single T-joists sections, in order that the distribution of bending moments across the slab will be clear and automatically taken into account as part of TCC design.

Further work is required to characterise the behaviour of TCC floor specimens that have a less-dense shear connector arrangement, allowing the specimen to more fully take advantage of the ductility

offered by the connections before failure. For future tests on multi-joist TCC floors, the through-depth strain gauge layout should be used in order to determine individual T-section moment values and hence transverse sharing, so as to grow the body of research which utilises this method. In the longer term, the development of an experimentally-underpinned database of transverse sharing of longitudinal moments in multi-joist TCC floors under different realistic load forms could enable more structurally efficient design of such floors in future practice.

## 5 Acknowledgements

The authors are grateful to the Institution of Structural Engineers who sponsored this work as part of the IStructE Research Award 2016. (https://www.istructe.org/events-awards/research-award)

## 6 References

[1] British Standards Institution, (2004) 'BS EN 1995-1-1:2004. Eurocode 5: Design of timber structures — Part 1-1: General — Common rules and rules for buildings' London, British Standards Institution.

[2] Meierhofer, U., (1993) 'A Timber-Concrete Composite System' Structural Engineering International **2/93** pp. 104-107.

[3] Khorsandnia, N., Valipour, H. R., Crews, K., (2012) 'Experimental and analytical investigation of short-term behaviour of LVL–concrete composite connections and beams' *Construction and Building Materials* **37** pp. 229-238.

[4] Negrao, J., De Oliviera, C. A. L., De Oliviera, F. M. M., Cachim, P. B., (2010) 'Glued Composite Timber-Concrete Beams.II - Analysis and Tests of Beam Specimens' *Journal of Structural Engineering* **136**(10) pp. 1246-1254.

[5] Persaud, R., Symons, D., (2006) 'Design and testing of a composite timber and concrete floor system' *The Structural Engineer* **84**(4) pp. 22-30.

[6] Rijal, R., Samali, B., Shrestha, R., Crews, K., (2015) 'Experimental and analytical study on dynamic performance of timber-concrete composite beams' *Construction and Building Materials* **75** pp. 46-53.

[7] Schanack, F., Ramos, O. R., Reyes, J. P., Low, A. A., (2015) 'Experimental study on the influence of concrete cracking on timber concrete composite beams' *Engineering Structures* **84** pp. 362-367.

[8] Yeoh, D., Fragiacomo, M., Carradine, D., (2013) 'Fatigue behaviour of timber-concrete composite connections and floor beams' *Engineering Structures* **56** pp. 2240-2248.

[9] Sebastian, W. M., Mudie, J., Cox, G., Piazza, M., Tomasi, R., Giongo, I., (2016) 'Insight into mechanics of externally indeterminate hardwood–concrete composite beams' *Construction and Building Materials* **102**(2) pp. 1029-1048.

[10] Monteiro, S. R. S., (2015). 'Load Distribution on Timber-Concrete Composite Floors' PhD Thesis, University of Coimbra, Coimbra.

[11] Kieslick, H., Holschemacher, K., (2016). 'Transversal load sharing in timber-concrete floors - experimental and numerical investigations' *Proceedings of the 14th World Conference on Timber Engineering,* Vienna, Austria.

[12] Blesak, L., Monteiro, S. R. S., Dias, A.M.P.G., Wald, F., (2016) 'Transverse loading distribution related to micro-cracks evolution on a timber-concrete slab' Wood research **61**(3) pp. 385-398.

[13] Dias, A. M. P. G., Monteiro, S. R. S., Martins, C., (2013) 'Reinforcement of timber floors - transversal load distribution on timber-concrete systems' Advanced Materials Research **778** pp. 657-664.

[14] Monteiro, S. R. S., Dias, A. M. P. G., Lopes, S., (2016) 'Transverse distribution of internal forces in timber-concrete floors under external point and line loads' Construction and Building Materials **102**(2) pp. 1049-1059.

[15] Gutkowski, R. M., Balogh, J., Brown, K., Koike, E., Etournaud, P., (2000) 'Laboratory tests of composite wood-concrete beam and floor specimens' Proceedings of the 6th World Conference on Timber Engineering, Whistler, Canada

[16] Kieslich, H., Holschemacher, K., (2014) 'Investigations on load sharing effects in timber-concrete composite constructions' Proceedings of the 9th International Conference on Structural Analysis of Historical Constructions, Mexico City, Mexico.

[17] Ceccotti, A., Fragiacomo, M., Giordano, S., (2006) 'Behaviour of a Timber-Concrete Composite Beam with Glued Connection at Strength Limit State' Proceedings of the 9th World Conference on Timber Engineering, Portland, USA.

[18] Boccadoro, L., Frangi, A., (2013) 'Experimental Analysis of the Structural Behavior of Timber-Concrete Composite Slabs made of Beech-Laminated Veneer Lumber' Journal of Performance of Constructed Facilities **28**(6)

[19] Bajzecerova, V., (2017) 'Bending Stiffness of CLT-Concrete Composite Members - Comparison of Simplified Calculation Methods' Procedia Engineering **190** pp. 15-20.

[20] Deam, B. L., Fragiacomo, M., Buchanan, A. H., (2008) 'Connections for composite concrete slab and LVL flooring systems' Materials and Structures **41** pp. 495-507.

[21] Ollgard, J. G., Slutter, R. G., Fisher, J. W., (1971) 'Shear strength of stud connectors in lightweight and normal weight concrete' AISC Engineering Journal pp. 55-64.

664 [22] Dias, A. M. P. G., Martins, C. E. J., (2012) 'Mechanical performance of a new, more
665 environmentally friendly, timber-concrete connection' Proceedings of the 12th World Conference on
666 Timber Engineering, Auckland, New Zealand.

667 [23] Sebastian, W. M., Thompson, S., (2012) 'Indicative comparisons between bonded and
668 dowelled hardwood studs for limecrete-spruce connections' Engineering Structures **45** pp. 151-165.

669 [24] Miotto, J. L., Dias, A. A., (2015) 'Structural efficiency of full-scale timber-concrete
670 composite beams strengthened with fiberglass reinforced polymer' Composite Structures **128** pp. 145-
671 154.

672 [25] Jiang, Y., Hong, W., Hu, X., Crocetti, R., Wang, L., Sun, W., (2017) 'Early-age
673 performance of lag screw shear connections for glulam-lightweight concrete composite beams'
674 Construction and Building Materials **151** pp. 36-42.

675 [26] Symons, D., Persaud, R., Stanislaus, H., (2010) 'Strength of inclined screw shear
676 connections for timber and concrete composite construction' The Structural Engineer **88**(1) pp. 25-32.

677 [27] Dias, A. M. P. G., Cruz, H., Lopes, S., Van de Kuilen, J. W., (2010) 'Stiffness of dowel-
678 type fasteners in timber-concrete joints' Proceedings of the Institution of Civil Engineers - Structures
679 and Buildings **163**(SB4) pp. 257-266.

680 [28] Brunner, M., Romer, M., Schnuriger, M., (2007) 'Timber-concrete-composite with an
681 adhesive connector (wet on wet process)' Materials and Structures **40** pp. 119-126.

682 [29] Yeoh, D., Fragiacomo, M., De Franceschi, M.,Buchanan, A. H., (2011) 'Experimental
683 Tests of Notched and Plate Connectors for LVL-Concrete Composite Beams' Journal of Structural
684 Engineering **137**(2) pp. 261-269.

685 [30] Clouston, P., Bathon, L. A., Schreyer, A., (2005) 'Shear and Bending Performance of a
686 Novel Wood–Concrete Composite System' Journal of Structural Engineering **131**(9) pp. 1404-1412.

687 [31] Miotto, J. L., Dias, A. A., (2008) 'Glulam-concrete composite structures - experimental
688 investigation into the connection system' Proceedings of the 10th World Conference on Timber
689 Engineering, Miyazaki, Japan.

690 [32] Shan, B., Xiao, Y., Zhang, W., Liu, B., (2017) 'Mechanical behavior of connections for
691 glubam-concrete composite beams' Construction and Building Materials **143** pp. 158-168.

692 [33] Bathon, L. A., Clouston, P., (2004) 'Experimental and numerical results on semi
693 prestressed wood-concrete composite floor systems for long span applications' Proceedings of the 8th
694 World Conference on Timber Engineering, Lahti, Finland.

695 [34] British Standards Institution, (1991) 'BS EN 26891:1991. Timber structures. Joints made
696 with mechanical fasteners. General principles for the determination of strength and deformation
697 characteristics' London, British Standards Institution.

698 [35] British Standards Institution, (2004) 'BS EN 1991-1-1:2002. Eurocode 1: Actions on
699 structures — Part 1-1: General actions — Densities, self-weight, imposed loads for buildings' London,
700 British Standards Institution.